Supporting Information

Unlocking the Potential: Strategic Synthesis of a Previously Predicted Pyrazolate-Based Stable MOF with Unique Clusters and High Catalytic Activity

Xiang-Yu Li, Yan-Long Zhao, Su-Nan Chen, Kecheng Wang,* Shengjun Wang, Lin-Hua Xie,* and Jian-Rong Li*

Beijing Key Laboratory for Green Catalysis and Separation, Department of Chemical Engineering, College of Materials Science and Engineering, Beijing University of Technology, Beijing 100124, P. R. China.

*Corresponding author emails: kcwang@bjut.edu.cn; xielinhua@bjut.edu.cn; jrli@bjut.edu.cn

Experimental Section

General characterization

All general reagents (AR grade) were commercially available and as received. ^{1}H NMR data were collected on a Bruker Avance III HD 400 MHz NMR spectrometer. The power diffraction (PXRD) patterns were recorded on a Rigaku Smartlab3 X-ray powder diffractometer equipped with a Cu-sealed tube (λ = 1.54178 Å) at room temperature (RT). Gas adsorption/desorption isotherms were recorded using a Micrometrics ASAP 2020. Gas adsorption measurements were performed using ultra-high purity (99.99Metal contents of MOFs were determined by ICP-OES on an atomic emission spectrometer (OPTIMA7000DV, PE, AGILENT, America). Scanning electron micrographic (SEM) image was recorded on a scanning electron microscope (SEM Zeiss SUPRA 55).

Ligand synthesis

The pyrazole-based ligand 1,3,5-tris(1*H*-pyrazol-4-yl)benzene (H_3BTP) was obtained by a modified.[1]

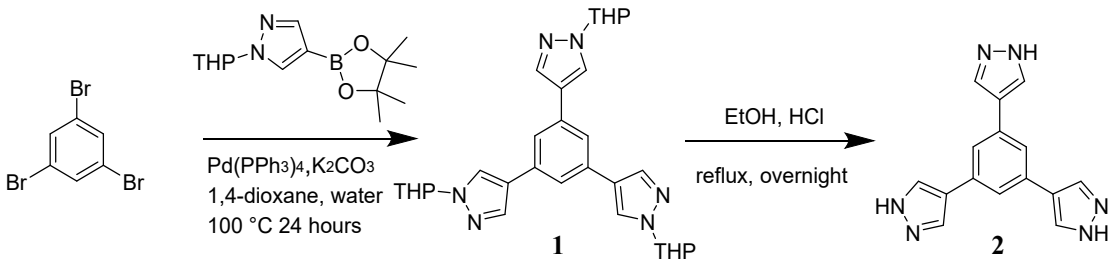

1,3,5-tris(1-(tetrahydro-2H-pyran-2-yl)-1H-pyrazol-4-yl)benzene 1,3,5-tribromobenzene (5.0 g, 15.9 mmol), tert-butyl-4-(4,4,5,5-tetramethyl-1,3,2-dioxaborolan-2-yl)-1H-pyrazole-1-carboxylate (20.0 g, 71.4 mmol) and K_2CO_3 (8.8 g, 63.6 mmol) were added to 1,4-dioxane (200 mL) and water (90 mL), and the mixture was deaerated under a nitrogen atmosphere for 15 minutes. $Pd(PPh_3)_4$ (1.8 g, 1.59 mmol) was added to the reaction mixture with stirring, and then the reaction mixture heated to 100 ℃ for 24 hours under nitrogen atmosphere. Then the solvent was removed and the residue was extracted with CH_2Cl_2 (300 mL) and water (300 mL), washed with water (300 mL × 3). The organic layer was dried with anhydrous $MgSO_4$, and the solvent was removed in a vacuum. The crude product was purified by column chromatography to obtain 1,3,5-tris(1-(tetrahydro-2H-pyran-2-yl)-1H-pyrazol-4-yl)benzene (**1**).

1,3,5-tris(1*H*-pyrazol-4-yl)benzene 1,3,5-tris(1-(tetrahydro-2H-pyran-2-yl)-1H-pyrazol-4-yl)benzene was dissolved in 2 M HCl/ethanol solution (200 mL) and refluxed overnight. Afterward, the solvent was removed by rotary evaporation. The residue was dispersed in 200 mL of water, and the PH was adjusted to 10 by slowly adding ammonium hydroxide. The resulting precipitate was collected via filtration, washed with water (100 mL × 3). The white solid 1,3,5-tris(1H-pyrazol-4-yl)benzene was obtained by drying under 80 ℃。

Synthesis of BUT-124(Cd)

BUT-124(Cd) was synthesized under solvothermal conditions. Initially, H_3BTP (0.06 mmol, 16 mg), $Cd(ClO_4)_2 \cdot 6H_2O$ (0.09 mmol, 36.8 mg), and ammonium hydroxide (150 μL) were ultrasonically dissolved in 4 mL of *N*, *N*-dimethylformamide (DMF) in a 20 mL Teflon-lined stainless-steel autoclave. The autoclave was heated at 80 ℃ for 4 h in an oven. After cooling to RT, the resulting white powder was harvested by filtration, washed with DMF, and then soaked in DMF.

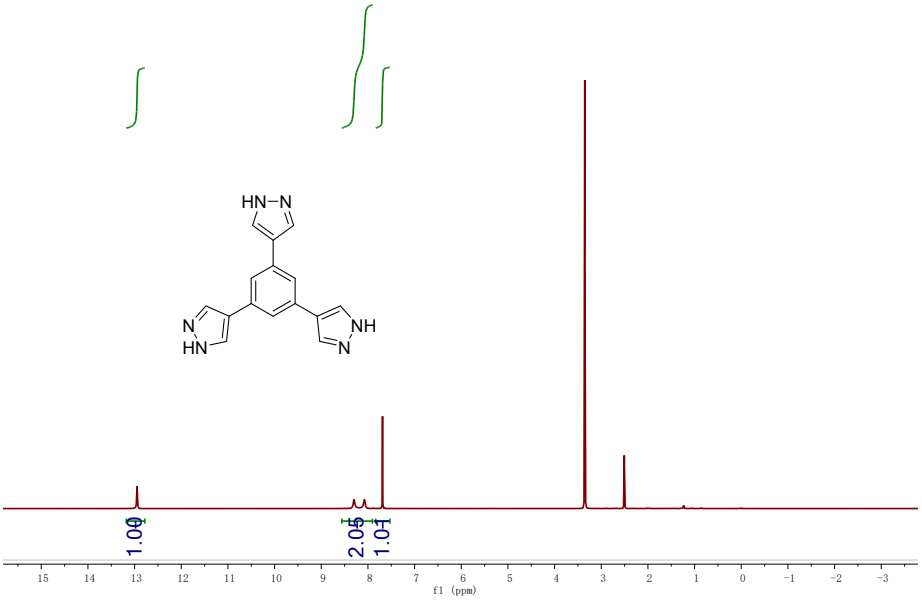

Figure S1 ^{1}HNMR spectrum of H_3BTP.

Synthesis of BUT-124(Co)-S80

The pre-synthesized **BUT-124(Cd)** samples (200 mg) were immersed into $Co(NO_3)_2 \cdot 6H_2O$ solutions (*N*,*N*-dimethylacetamide(DMA) as the solvent) of the concentration 10 mg/mL at RT, 60℃, 80℃ for 24 h, progressively. During this process, the $Co(NO_3)_2 \cdot 6H_2O$ solution was refreshed each 12 h (100 mL × 6), and the mixture was stirred. After the exchange, the reaction mixture was cooled to room temperature, and dark brown powder were harvested. The samples were wash with DMA, and then solvent-exchanged by methanol (MeOH). Dry the samples under reduced pressure to obtain product, named **BUT-124(Co)-S80** (yield: 188.2mg).

Sample activation

Before gas adsorption measurements, about 50 mg samples were soaked in 10 mL of *N*,*N*-dimethylformamide (DMF) for 1 day at RT. The samples were collected by decanting and then, they were soaked in 15 mL of methanol for another 3 days with fresh solvent exchanged every day. After solvent exchange, **BUT-124(Cd)** was loaded into a sample tube and further activated under high vacuum at 80 ℃ for 10 h, and **BUT-124(Co)-S80** was activated at 150 ℃ for 10 h.

Brunauer-Emmett-Teller (BET) surface areas

The Brunauer-Emmett-Teller (BET) theory is a widely used method for determining the specific surface area of

porous materials, including metal-organic frameworks (MOFs).[2, 3] The BET equation relates the amount of adsorbed gas on a material's surface to its surface area. The BET surface areas of **BUT-124** series were evaluated by nitrogen adsorption isotherms at 77 K.

The BET equation was given by:

$$\frac{v}{(\frac{P}{P_0})(1-\frac{P}{P_0})} = \frac{c-1}{c}\frac{v_m}{P_0} + \frac{v_m - v}{c}$$

Here, v is the volume of gas adsorbed at relative pressure P/P_0, v_m is the volume of gas adsorbed when the surface is fully covered, and c is a constant related to the energy of adsorption. The BET equation required a mathematical transformation to linearize it by plotting $\frac{v}{(\frac{P}{P_0})(1-\frac{P}{P_0})}$ against P/P_0 and fitting a straight line to the linear portion. From the slope (K) and intercept (I) of the linearized BET plot (Figure S10-S21), we can calculate the BET surface area (A_{BET}) using the formula:

$$A_{BET} = \frac{N_A \partial}{22414(K+I)}$$

Where:

N_A is the Avogadro's constant, ∂ is the cross-sectional area of adsorbed nitrogen molecule, usually taken as 0.162 nm^2, and 22414 is the volume (ml) of 1 mol of gas in the standard temperature and pressure.

Take **BUT-124(Cd)** as an example, the detailed calculation of surface areas was as follows.

$$A_{BET} = 6.023\times10^{23}\times0.162\times10^{-18}/(22414\times(0.00278 + 4.09688E\text{-}6)) = 1563.6\ m^2\ g^{-1}$$

Accordingly, the BET surface areas of **BUT-124(Co)-RT**, **BUT-124(Co)-60**, **BUT-124(Co)-80**, **BUT-124(Co)-S60**, **BUT-124(Co)-S80** are 439.5, 1268.8, 1623.1, 1326.4 and 1635.4 $m^2\ g^{-1}$, respectively.

Pore size distribution calculation

Pore size distribution calculations were performed on the N_2 adsorption isotherm data using the density functional theory (DFT) model. The total experimental isotherms are used to determine the microporosity and medium porosity as the continuous distribution of pore volume with respect to pore size. Pore size distributions of **BUT-124(Cd)** and **BUT-124(Co)-S80** were shown in Figure S6.

Stability test

Stability is one of the primary concerns for the OER application of MOFs. To examine the chemical stability of Cd-BTP-80, the as-synthesized samples (50 mg) were exposed in air, and soaked in water, 1 M KOH and saturate NaOH solution at RT 24 h, respectively. Then the treated samples were collected by decanting and washed with water and methanol for PXRD measurement and N_2 adsorption.

Details for Pawley refinement

The initial structure for $Cu_3(BTP)_2$ was referred to the reported work (CCDC identifier: 804990).[4] The XRD data of

BUT-124(Cd) samples were analyzed by using Topas V4.2 and Pawley method.[5] The range of the data was 2θ = 4 ° - 90 °, the fitting quality index Rwp = 2.86%, and GOF (goodness of fit) = 2.84. The analysis confirmed that the **BUT-124(Cd)** sample was cubic structure and the space group was $Pm\bar{3}m$ The cell parameter a = 19.505(69) å was obtained by refinement optimization. Unit cell parameters and fitting reliability were listed in Table S1.

Preparation of working electrode

The powder coated on a Co foil (1 cm × 2 cm × 0.001 cm) using Nafion as binder: a suspension was prepared by dispersing MOF powder (10 mg) in a mixed solution (2 mL) containing N-methylpyrrolidone (NMP) (1.9 mL) and a 5 wt% Dupont Nafion 117 solution (0.1 mL), following by ultrasonication for 30 min. Subsequently, 10 μL of above solution was uniformly spread onto a clean Co foil (1 cm^{-2}). The working electrode was dried at ambient temperature before electrochemical measurements.

Purification of KOH electrolyte

A trace amount of Fe is expected to be present in unpurified KOH solution. KOH electrolyte was purified using a method reported.[6,7] 2 g of $Ni(NO_3)_2 \cdot 6H_2O$ were dissolved in 4 mL of deionized (DI) water to prepare a clear solution. This solution was subsequently added to 20 milliliters of 1 M potassium hydroxide (KOH), precipitating $Ni(OH)_2$. The $Ni(OH)_2$ precipitate was then carefully washed with DI water through a process of redispersion, centrifugation to pellet the solid, and decanting to remove the supernatant liquid, ensuring the removal of any soluble impurities. The washed $Ni(OH)_2$ was next redispersed in 40 mL of 1 M KOH and stirred for 30 minutes to achieve a uniform suspension. The mixture was then set aside to rest for 6 hours to allow for complete settling of the $Ni(OH)_2$. After the resting period, the supernatant liquid was collected and subjected to thorough centrifugation to separate any remaining solid particles. Finally, the supernatant, which consisted of pure KOH free from $Ni(OH)_2$, was carefully collected and utilized for electrochemical measurements, ensuring that the conditions for these measurements were well-controlled and free from interferences.

Electrochemical measurements

Electrochemical performances were measured in a three-electrode setup using a Zennium electrochemistry workstation with an electrolyte solution of 1.0 M KOH. The Cu foil were employed as the working electrode, and the Ag/AgCl (saturated KCl) electrode and platinum plate were used as the reference and counter electrodes, respectively. The potentials reported in the work were calibrated to reversible hydrogen electrode (RHE) according to the Nernst equation: $E_{RHE} = E_{Ag/AgCl} + 0.197 + 0.059pH$ (pH = 14). The linear scan voltammetry (LSV) was performed at a scan rate of 5 mV/s. The cyclic voltammogram (CV) was recorded with a scan rate of 100 mV/s. Electrochemical impedance spectroscopy (EIS) was measured from 10^5 to 0.01 Hz.

Computational method

In the alkaline solution, the overall OER reaction was:

$4OH^- \rightarrow O_2 + 2H_2O + 4e^-$

And the electrocatalytic OER process include four elementary steps:

$OH^- + * \rightarrow OH^* + e^-$

$OH^- + OH^* \rightarrow O^* + H_2O + e^-$

$OH^- + O^* \rightarrow OOH^* + e^-$

$OH^- + OOH^* \rightarrow O_2 + H_2O + e^- + *$

We have employed the Vienna Ab Initio Package (VASP)[8,9] to perform all the density functional theory (DFT) calculations within the generalized gradient approximation (GGA) using the PBE[10] formulation. We have chosen the projected augmented wave (PAW) potentials[11,12] to describe the ionic cores and take valence electrons into account using a plane wave basis set with a kinetic energy cutoff of 400 eV. Partial occupancies of the Kohn−Sham orbitals were allowed using the Gaussian smearing method and a width of 0.05 eV. The electronic energy was considered self-consistent when the energy change was smaller than 10^{-5} eV. A geometry optimization was considered convergent when the force change was smaller than 0.02 eV/Å. Grimme's DFT-D3 methodology[13,14] was used to describe the dispersion interactions.

The **BUT-124(Co)-S80** unit cell was used for all the calculations. One H_2O molecule on Co was removed in order to let the Co atom be the adsorption site. During structural optimizations, the gamma point in the Brillouin zone was used for k-point sampling, and all atoms were allowed to relax.

The free energy of a gas phase molecule or an adsorbate on the surface was calculated by the equation G = E + ZPE − TS, where E is the total energy, ZPE is the zero-point energy, T is the temperature in kelvin (298.15 K is set here), and S is the entropy.

Results and Discussion

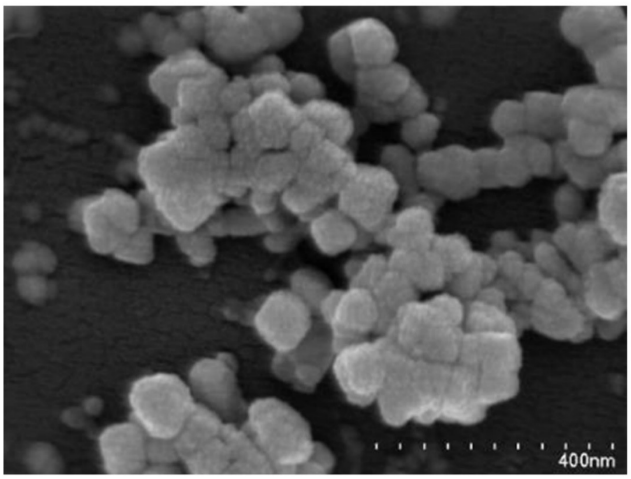

Figure S2 SEM image of the **BUT-124(Cd)**.

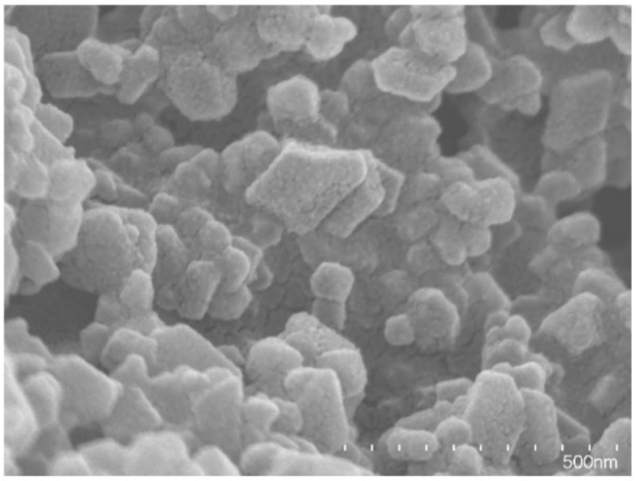

Figure S3 SEM image of **BUT-124(Co)-S80**.

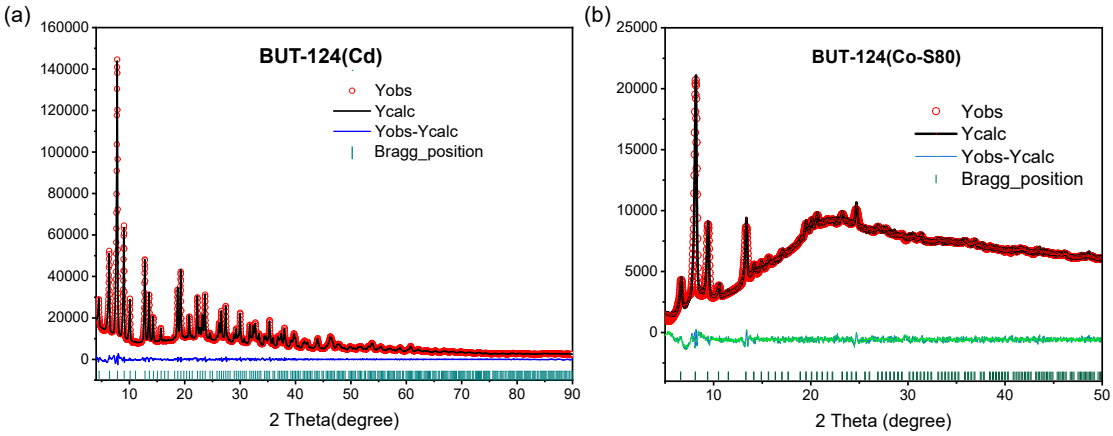

Figure S4 Pawley method fit to PXRD for (a) **BUT-124(Cd)** and (b) **BUT-124(Co)-S80**

Table S1. The pattern matching analysis data for **BUT-124(Cd)** and **BUT-124(Co)-S80** by the Pawley method.

	BUT-124(Cd)	**BUT-124(Co)-S80**
Initial lattice parameters	a = 18.807 (76) Å	a = 18.807 (76) Å
	b = 18.807 (76) Å	b = 18.807 (76) Å
	c = 18.807 (76) Å	c = 18.807 (76) Å
	α = 90°	α = 90°
	β = 90°	β = 90°
	γ = 90°	γ = 90°
	V = 6652.11 Å^3	V = 6652.11 Å^3
Fitted lattice parameters	a = 19.505 (69) Å	a = 18.795 (15) Å
	b = 19.505 (69) Å	b = 18.795 (15) Å
	c = 19.505 (69) Å	c = 18.795 (15) Å
	α = 90°	α = 90°
	β = 90°	β = 90°
	γ = 90°	γ = 90°
	V = 7421.68 Å^3	V = 6640.04 Å^3
R_p	2.07%	1.08%
R_{wp}	2.86%	1.81%

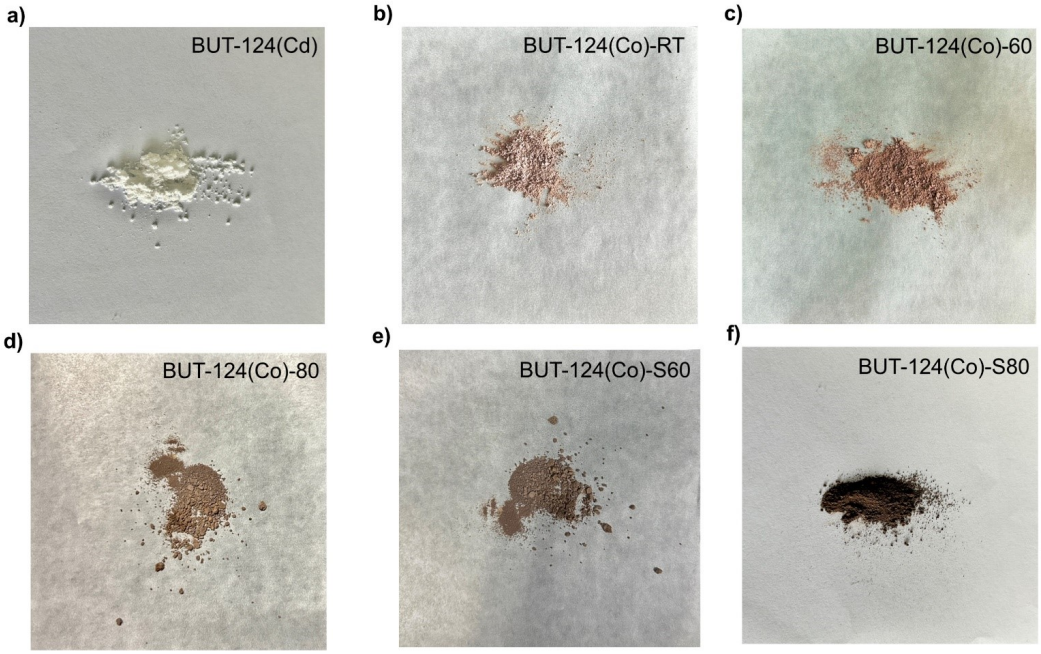

Figure S5 a) Photograph of the as-synthesized **BUT-124(Cd)** sample. b-f) the color change of the samples after metal metathesis.

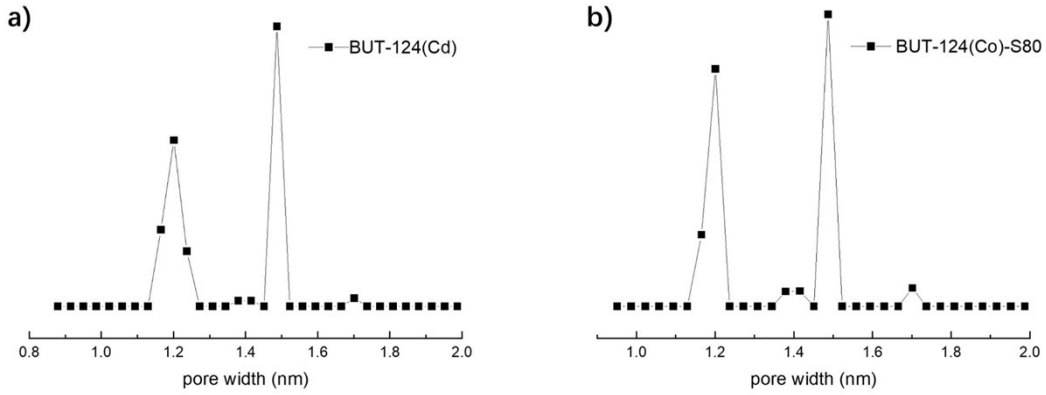

Figure S6 Pore size distribution profile of **BUT-124(Cd)** and **BUT-124(Co)-S80**.

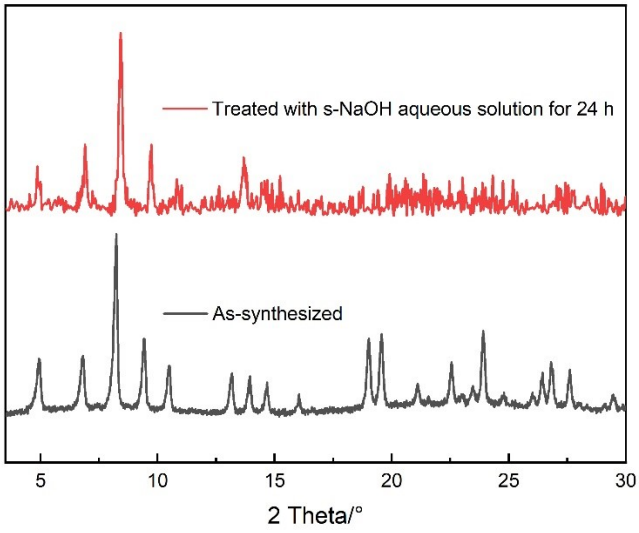

Figure S7 PXRD patterns for **BUT-124(Co)-S80** samples after being treated with saturated aqueous NaOH solution (s-NaOH).

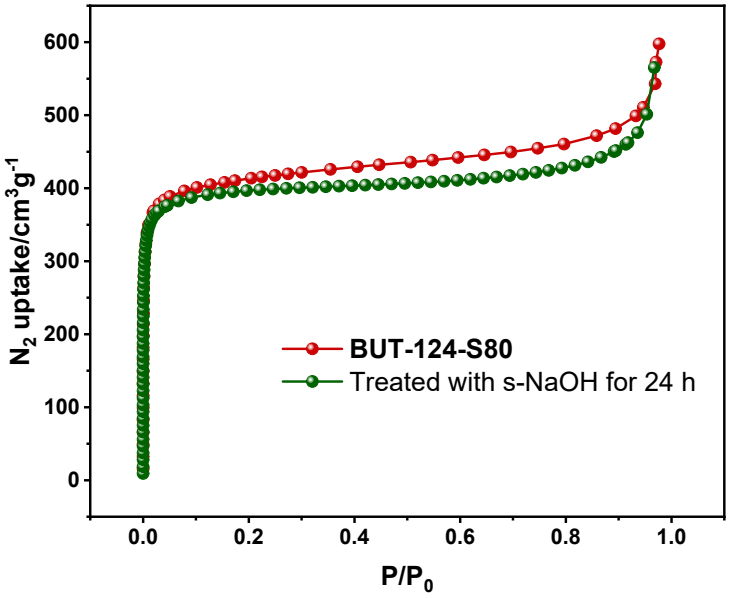

Figure S8 N_2 adsorption isotherms recorded at 77 K for **BUT-124(Co)-S80** and its sample after treated by saturated aqueous solution of NaOH (s-NaOH) for 24 hours.

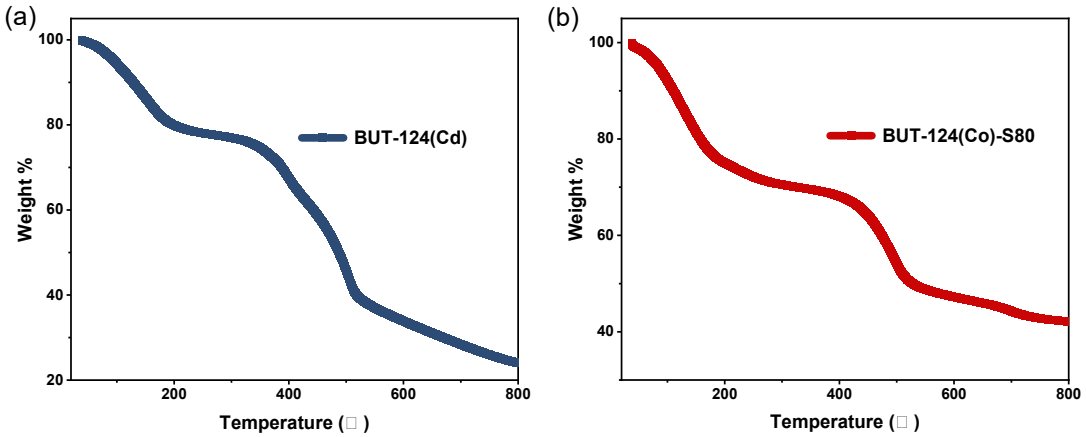

Figure S9 TGA curves of **BUT-124(Cd)** and **BUT-124(Co)-S80**.

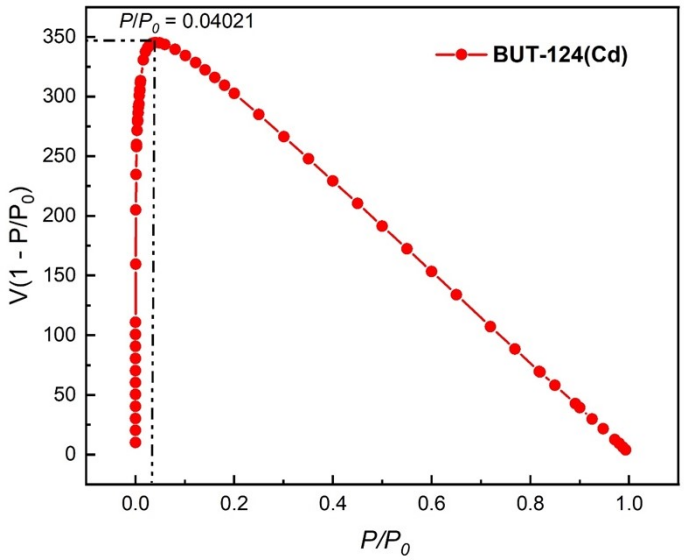

Figure S10 The consistency plot for **BUT-124(Cd).**

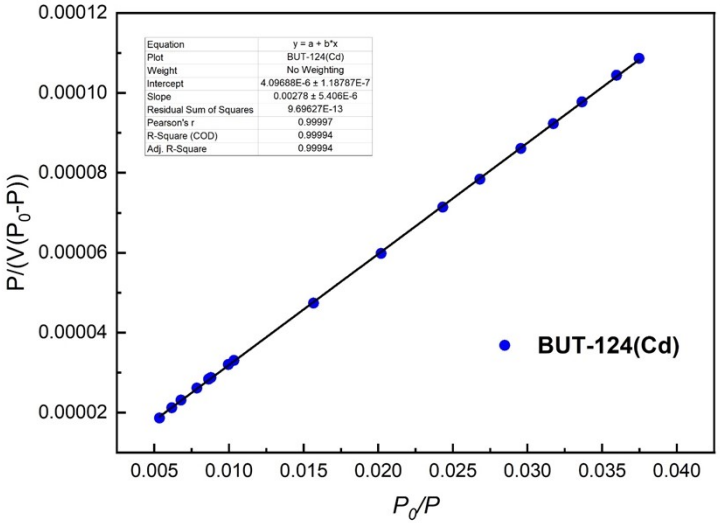

Figure S11 The calculation of surface areas for **BUT-124(Cd).**

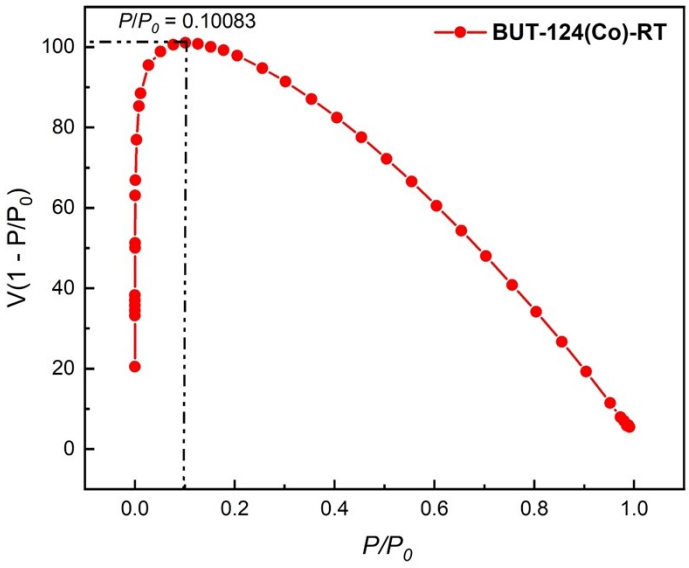

Figure S12 The consistency plot for **BUT-124(Co)-RT.**

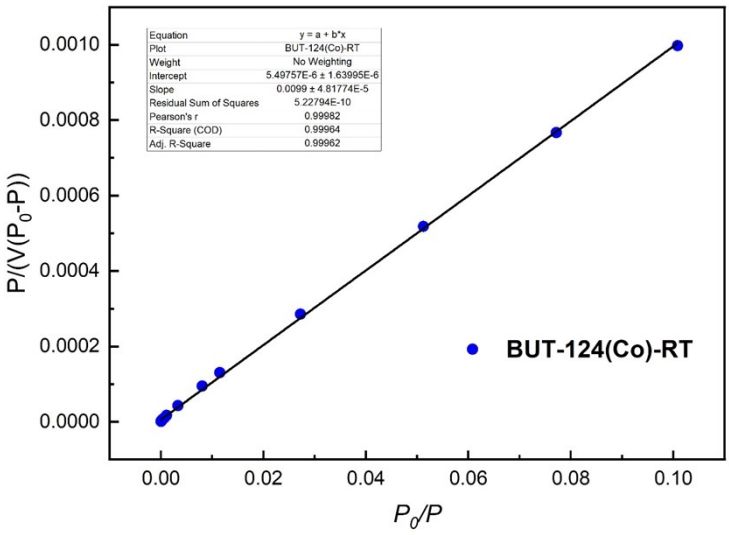

Figure S13 The calculation of surface areas for **BUT-124(Co)-RT.**

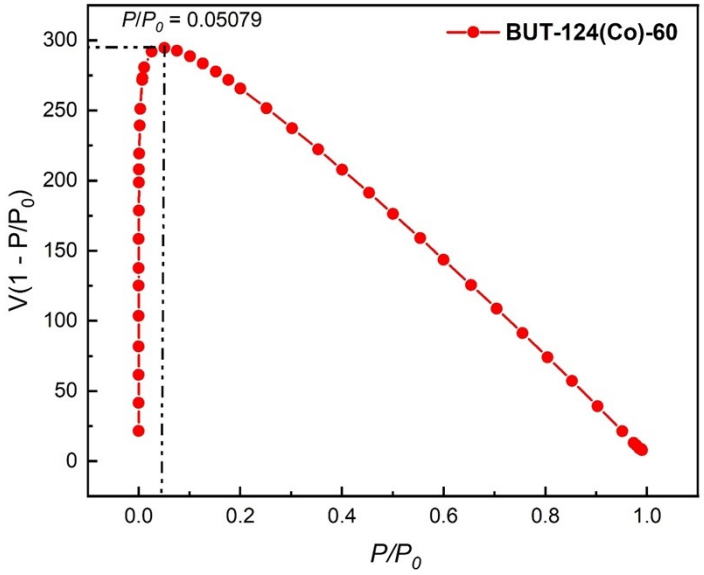

Figure S14 The consistency plot for **BUT-124(Co)-60.**

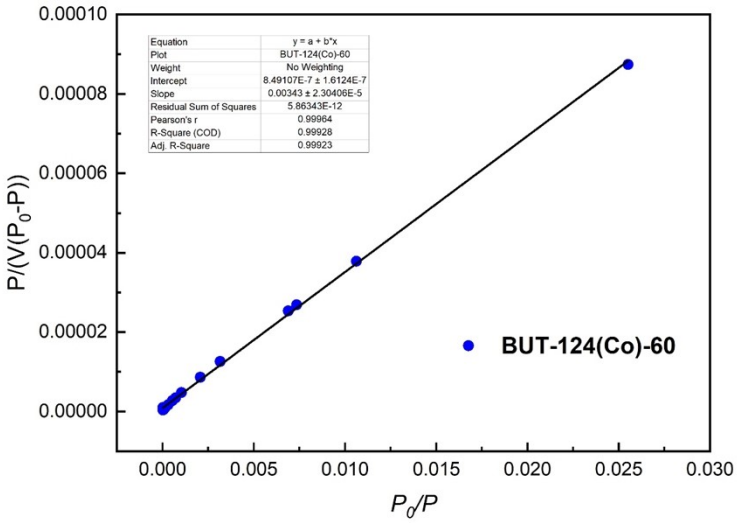

Figure S15 The calculation of surface areas for **BUT-124(Co)-60.**

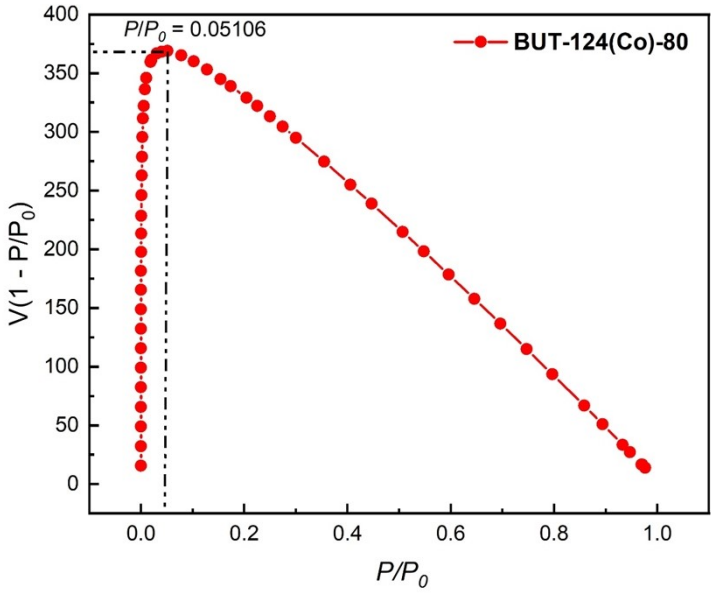

Figure S16 The consistency plot for **BUT-124(Co)-80.**

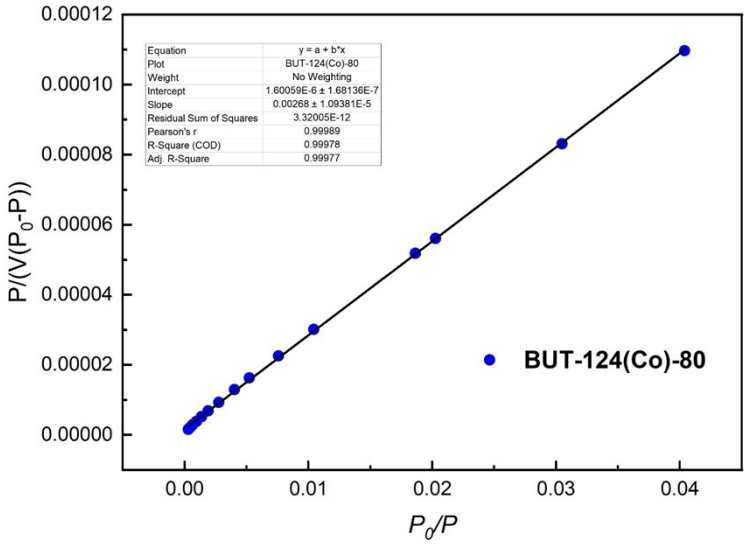

Figure S17 The calculation of surface areas for **BUT-124(Co)-80.**

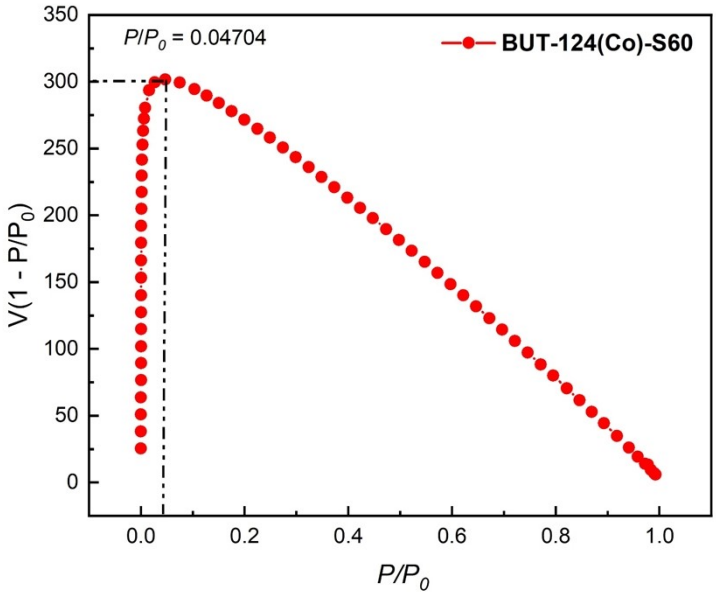

Figure S18 The consistency plot for **BUT-124(Co)-S60.**

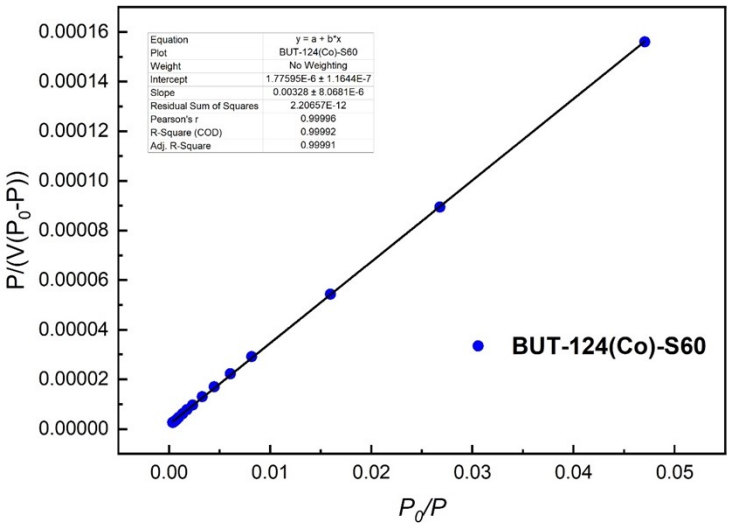

Figure S19 The calculation of surface areas for **BUT-124(Co)-S60**

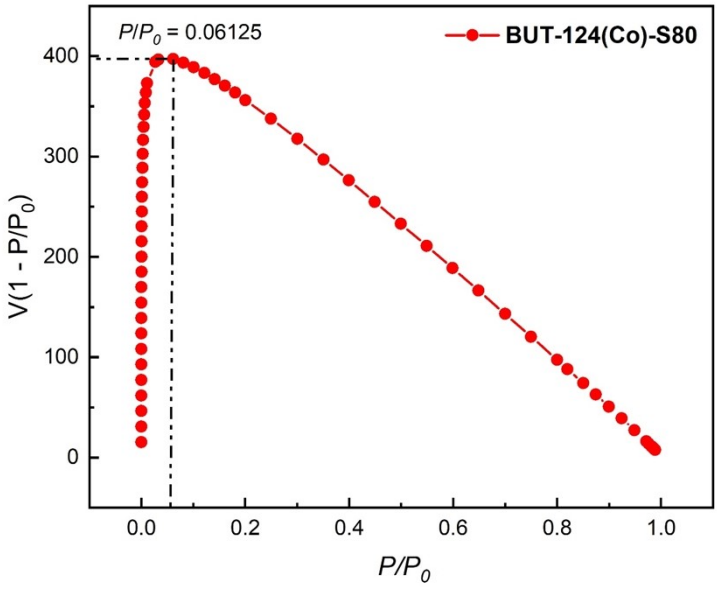

Figure S20 The consistency plot for **BUT-124(Co)-S80.**

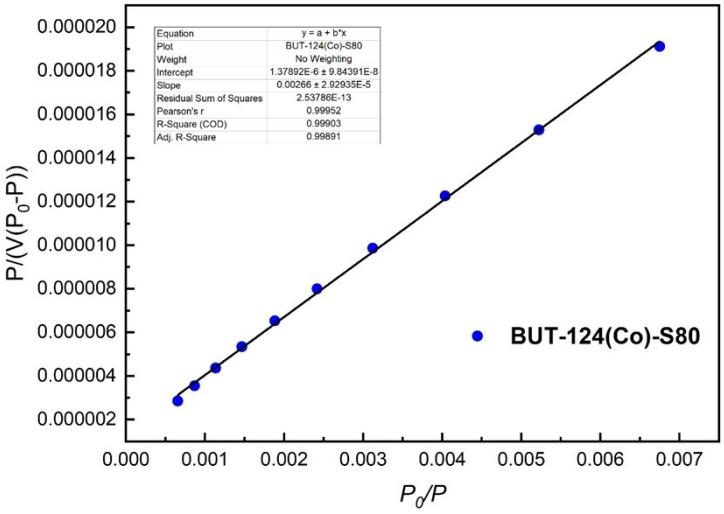

Figure S21 The calculation of surface areas for **BUT-124(Co)-S80.**

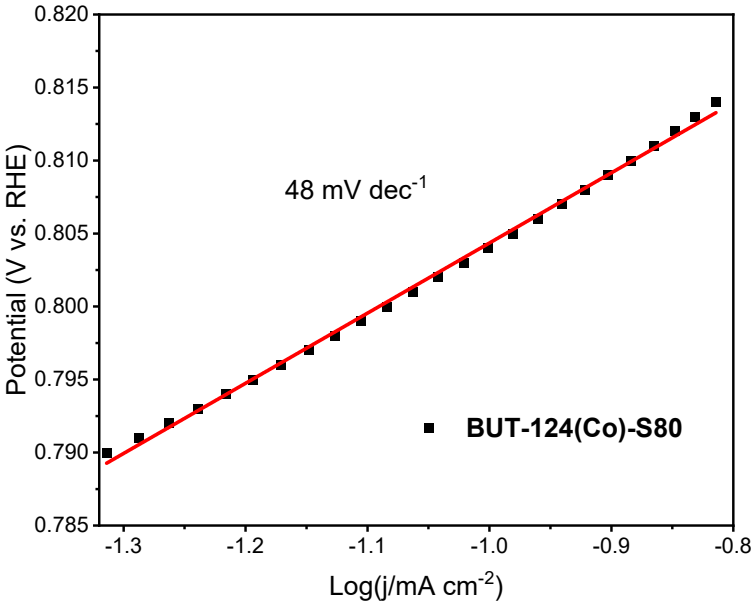

Figure S22 Tafel plot of **BUT-124(Co)-S80.**

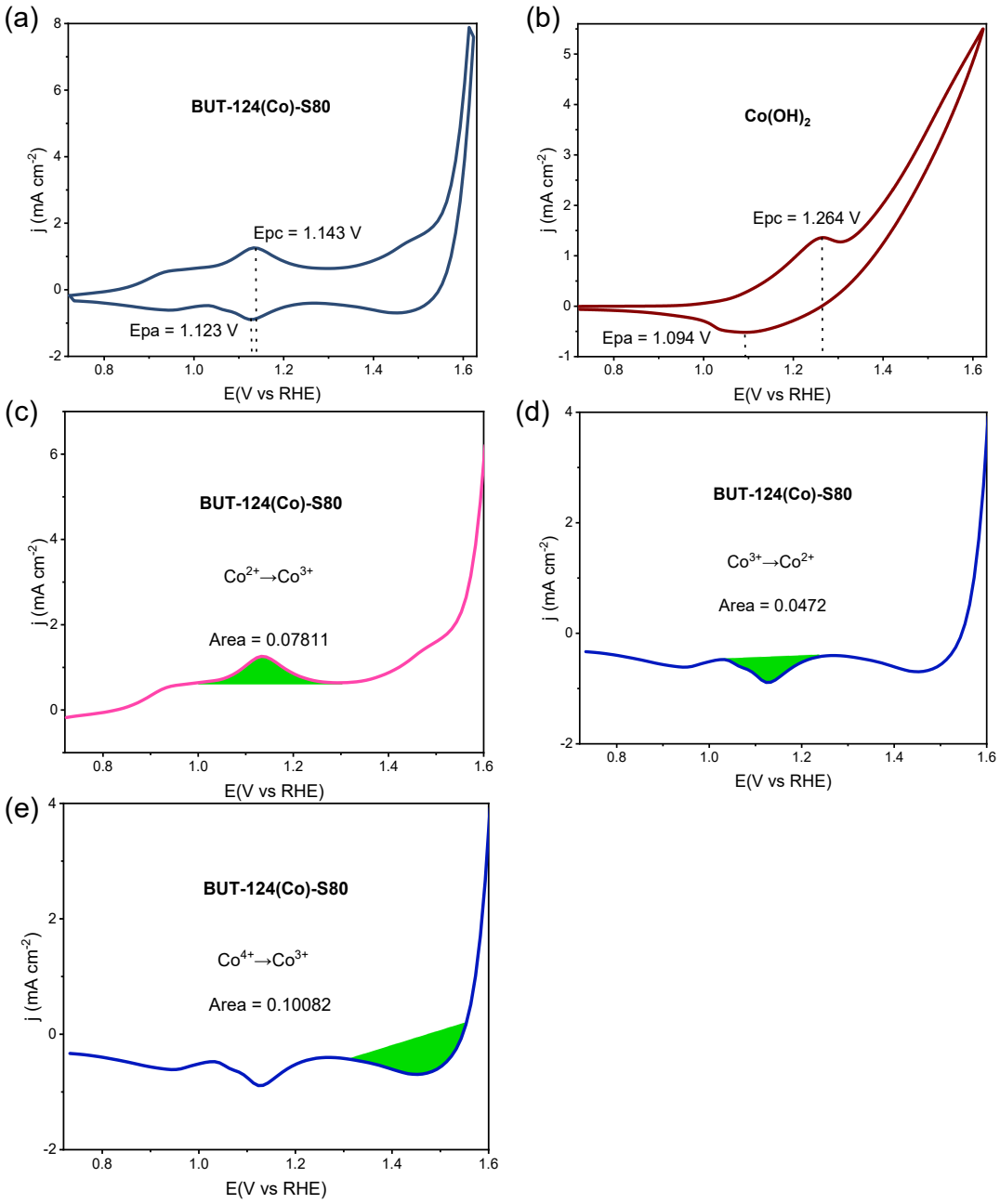

Figure S23 (a) CV graph of **BUT-124(Co) -S80**, (b) CV graph of $Co(OH)_2$, (c, d, e) calculation of the area under the oxidation and reduction peaks for **BUT-124(Co)-S80**.

<u>Calculation for Co^{2+} sites:</u>

(1) Area under oxidation peak (Co^{2+} to Co^{3+}) = 0.07811 V mA

Charge (Q) = 0.07811 V mA / 0.05 V s^{-1} = 1.5622 mA s = 1.5622 × 10^{-3} C

Since, Co^{2+} to Co^{3+} oxidation is one-electron transfer reaction,

The number of electrochemically accessible Co^{2+} = 1.5622 × 10^{-3} C / 1.602 × 10^{-19} C = 9.752 × 10^{15}

(2) Area under reduction peak (Co^{3+} to Co^{2+}) = 0.0472 V mA

Charge (Q) = 0.0472 V mA / 0.05 V s^{-1} = 0.944 mA s = 9.44 × 10^{-4} C

Since, Co^{3+} to Co^{2+} reduction is one-electron transfer reaction,

The number of electrochemically accessible $Co^{2+} = 9.44 \times 10^{-4}$ C / 1.602×10^{-19} C = 5.893×10^{15}

(3) Integration of redox peaks including both the oxidation and reduction peaks.

$(9.752 \times 10^{15} + 5.893 \times 10^{15})/2 = 7.823 \times 10^{15}$

The number of electrochemically accessible Co^{2+} is 7.823×10^{15}

Calculation for Co^{3+} sites:

Note: Only reduction peak is used for the Co^{3+}calculation. The oxidation peak pertaining Co^{3+} to Co^{4+} is not used for calculation as the OER current density overlaps with Co^{3+} to Co^{4+} peak.

Area under reduction peak (Co^{4+} to Co^{3+}) = 0.10082 V mA

Charge (Q) = 0.10082 V mA / 0.05 V s^{-1} = 2.0164 mA s = 2.0164×10^{-3} C

Since, Co^{4+} to Co^{3+} reduction is one-electron transfer reaction,

The number of electrochemically accessible $Co^{3+} = 2.0164 \times 10^{-3}$ C / 1.602×10^{-19} C = 1.259×10^{16}

The ratio of $Co^{2+}/Co^{3+} = 7.823 \times 10^{15}/1.259 \times 10^{16} \times 100\% = 62.3\%$

Table S2. Condition screening for accessing **BUT-124(Co)** from the template **BUT-124(Cd)** via metathesis. The samples were washed three times by DMA and three times by methanol. The samples were dried in 65 ° C oven and tested by PXRD.

Temp. (℃)	Time (d)	Metal salt	Conc.	Solvent	Results
RT	1	$CoCl_2$	10 mg/mL	DMF	Lose crystallinity
				DMA	Lose crystallinity
				MeOH	Lose crystallinity
				acetone	Lose crystallinity
RT	2	$CoCl_2$	10 mg/mL	DMF	Lose crystallinity
				DMA	Lose crystallinity
				MeOH	Lose crystallinity
				acetone	Lose crystallinity
RT	1	$Co(NO_3)_2$	10 mg/mL	DMF	Lose crystallinity
				DMA	Lose crystallinity
				MeOH	Lose crystallinity
				acetone	Lose crystallinity
RT	2	$Co(NO_3)_2$	10 mg/mL	DMF	Lose crystallinity
				DMA	24% exchange
	2	$Co(NO_3)_2$	10 mg/mL	MeOH	Lose crystallinity
				acetone	Lose crystallinity
60	1	$CoCl_2$	10 mg/mL	DMA	Lose crystallinity
				MeOH	Lose crystallinity
				acetone	Lose crystallinity
60	2	$CoCl_2$	10 mg/mL	DMF	Lose crystallinity
				DMA	Lose crystallinity
				MeOH	Lose crystallinity
				acetone	Lose crystallinity
60	1	$Co(NO_3)_2$	10 mg/mL	DMF	Maintain crystallinity
				DMA	Maintain crystallinity
				MeOH	Lose crystallinity
				acetone	Lose crystallinity
60	2	$Co(NO_3)_2$	10 mg/mL	DMF	Maintain crystallinity
				DMA	Maintain crystallinity 88% exchange

Temp. (℃)	Time (d)	Metal salt	Conc.	Solvent	Results
60				MeOH	Lose crystallinity
				acetone	Lose crystallinity
80	2	$Co(NO_3)_2$	10 mg/mL	DMA	90% exchange
100	2	$Co(NO_3)_2$	10 mg/mL	DMA	92% exchange

Table S3. ICP-AES data of the active **BUT-124(Co)** series.

	Exchange ratio	Condition
BUT-124(Co)-RT	25%	RT, 2 d
BUT-124(Co)-60	72%	60 ℃, 2 d
BUT-124(Co)-80	90%	80 ℃, 2 d
BUT-124(Co)-S60	81%	RT 1d + 60 1d
BUT-124(Co)-S80	95%	RT 1d + 60 1d +80 1d

Table S4. Comparison of the OER activities of MOFs and reported highly active inorganic catalysts supported in strong alkaline conditions.

Catalysts	η_{10} (mV)	Substrate	Electrolyte	Stability(h)	Ref.
BUT-124(Co)-S80	393	Co foil	1 M KOH	20	**This work**
NNU-21	555	Carbon cloth	0.1 M KOH	15	15
NNU-22	376	Carbon cloth	0.1 M KOH	15	
NNU-23	365	Carbon cloth	0.1 M KOH	15	
NNU-24	522	Carbon cloth	0.1 M KOH	15	
IrO_2	390	Carbon cloth	0.1 M KOH	-	
UTSA-16	408	GCE	1 M KOH	7	16
MAF-X27-OH	387	GCE	1 M KOH		17
	292*	Cu foil	1 M KOH	24	
$Co(OH)_2$	421	Carbon cloth	1 M KOH	-	
Co_3O_4	445	Carbon cloth	1 M KOH	-	
Co-WOC-1	390 at 1 mA cm^{-2}	GCE	0.1 M KOH	(1000 cycle)	18
FeTPyP-Co	351 at 1 mA cm^{-2}	Au	0.1 M NaOH	(15 cycle)	19

Catalysts	η_{10} (mV)	Substrate	Electrolyte	Stability(h)	Ref.
Co-ZIF-9	510 at 1 mA cm^{-2}	FTO glass	0.1 M KOH	25	20
PDA-MOF-0.1	350	Pt foil	0.1 M KOH	7	21
$Co_3(HITP)_2$	254	Carbon cloth	1 M KOH	12	22
Sq-zbr-MOF	230	Carbon paper	1 M KOH	15	23
CUMSs-ZIF-67	410	GCE	1 M KOH	24	24
$Ni_{0.75}Fe_{0.25}BDC$	310	GCE	1 M KOH	11.1	25
$Co_2(OH)_2BDC$	263	GCE	1 M KOH	3.3	26

*This value is obtained by placing the matrix in the reaction system for synthesizing MAF-X27-Cl, directly growing MOF crystals on the copper foil (hereinafter referred to as MAF-X27-OH(Cu)), and then subjecting it to ion exchange treatment.

Reference

1 Z. Wang, A. Bilegsaikhan, R. T. Jerozal, T. A. Pitt and P. J. Milner, *ACS Appl. Mater. Inter.*, 2021, **13**, 17517-17531.

2 Ambroz, F., Macdonald, T. J., Martis, V., Parkin, I. P., *Small Methods*, 2018, **2**, 1800173.

3 T. Xu, Z. Jiang, P. Liu, H. Chen, X. Lan, D. Chen, L. Li and Y. He, *ACS Appl. Nano Mater.*, 2020, **3**, 2911-2919.

4 V. Colombo, S. Galli, H. J. Choi, G. D. Han, A. Maspero, G. Palmisano, N. Masciocchi and J. R. Long, *Chem. Sci.*, 2011, **2**, 1311-1319.

5 A. Coelho, *J. Appl. Crystallog.*, 2018, **51**, 210-218.

6 V. Colombo, S. Galli, H. J. Choi, G. D. Han, A. Maspero, G. Palmisano, N. Masciocchi, J. R. Long, *Nano Energy*, 2021, 80, 105514.

7 L. Liu, L. P. Twight, J. L. Fehrs, Y. Ou, D. Sun, S. W. Boettcher, *ChemElectroChem*, 2022, 9, e202200279.

8 G. Kresse and J. Furthmüller, *Comp. Mater. Sci.*, 1996, **6**, 15-50.

9 G. Kresse and J. Furthmüller, *Phys. Rev. B*, 1996, **54**, 11169-11186.

10 J. P. Perdew, K. Burke and M. Ernzerhof, *Phys. Rev. Lett.*, 1996, **77**, 3865-3868.

11 G. Kresse and D. Joubert, *Phys. Rev. B*, 1999, **59**, 1758-1775.

12 P. E. Blöchl, *Phys. Rev. B*, 1994, **50**, 17953-17979.

13 S. Grimme, J. Antony, S. Ehrlich and H. Krieg, *J. Chem. Phys*., 2010, **132**, 154104.

14 J. K. Nørskov, J. Rossmeisl, A. Logadottir, L. Lindqvist, J. R. Kitchin, T. Bligaard and H. Jónsson, *J. Phys. Chem. B*, 2004, **108**, 17886-17892.

15 X. L. Wang, L. Z. Dong, M. Qiao, Y. J. Tang, J. Liu, Y. Li, S. L. Li, J. X. Su and Y. Q. Lan, *Angew. Chem. Int. Ed.*, 2018, **57**, 9660-9664.

16 J. Jiang, L. Huang, X. Liu and L. Ai, *ACS Appl Mater Interfaces*, 2017, **9**, 7193-7201.

17 X. F. Lu, P. Q. Liao, J. W. Wang, J. X. Wu, X. W. Chen, C. T. He, J. P. Zhang, G. R. Li and X. M. Chen, *J. Am. Chem. Soc.*, 2016, **138**, 8336-8339.

18 P. Manna, J. Debgupta, S. Bose and S. K. Das, *Angew. Chem. Int. Ed.,* 2016, **55**, 2425-2430.

19 Wurster, D. Grumelli, D. Hötger, R. Gutzler and K. Kern, *J. Am. Chem. Soc.*, 2016, **138**, 3623-3626.

20 S. Wang, Y. Hou, S. Lin and X. Wang, *Nanoscale*, 2014, **6**, 9930-9934.

21 F. Shi, Z. Wang, K. Zhu, X. Zhu and W. Yang, *Electrochim. Acta*, 2022, **416**, 140273.

22 Xing, Y. Wang, P. Zhou, Y. Liu, Z. Wang, P. Wang, Z. Zheng, H. Cheng, Y. Dai and B. Huang, *Appl. Catal. B- Environ.*, 2020, **278**, 140293.

23 S. Kandambeth, V. S. Kale, D. Fan, J. A. Bau, P. M. Bhatt, S. Zhou, A. Shkurenko, M. Rueping, G. Maurin, O. Shekhah and M. Eddaoudi, *Adv. Energy Mater.*, 2023, **13**, 2202964.

24 L. Tao, C.-Y. Lin, S. Dou, S. Feng, D. Chen, D. Liu, J. Huo, Z. Xia and S. Wang, *Nano Energy*, 2017, **41**, 417-425.

25 Y. Hao, Q. Liu, Y. Zhou, Z. Yuan, Y. Fan, Z. Ke, C.-Y. Su and G. Li, *Energy Environ. Mater*.,2019, **2**, 18-21.

26 Y. Xu, B. Li, S. Zheng, P. Wu, J. Zhan, H. Xue, Q. Xu and H. Pang, *J. Mater. Chem. A*, 2018, **6**, 22070-22076.